Corrosion Science 222 (2023) 111431

Contents lists available at ScienceDirect

Corrosion Science

journal homepage: www.elsevier.com/locate/corsci

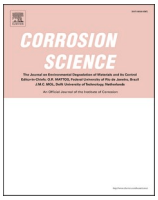

Stimulated corrosion damage of Ti-Al-N multilayer coatings under interval salt spray and hot condition

Dingwei Zhou [a,b], Zhenyu Wang [a,c,*], Yan Zhang [a], Jingjun Yan [a], Guanshui Ma [a], Xiaojun Hu [b], Peiling Ke [a,c], Aiying Wang [a,c,*]

[a] Key Laboratory of Marine Materials and Related Technologies, Zhejiang Key Laboratory of Marine Materials and Protective Technologies, Ningbo Institute of Materials Technology and Engineering, Chinese Academy of Sciences, Ningbo 315201, China
[b] College of Materials Science and Engineering, Zhejiang University of Technology, Hangzhou 310000, Zhejiang, China
[c] Ningbo Institute of Industrial Technology, Ningbo 315201, China

ARTICLE INFO

Keywords:
Ti-Al-N multilayered coating
PVD technique
Salt spray
Hot corrosion
Microstructure

ABSTRACT

Engines for marine are subjected to synergistic chloride corrosion and hot oxidation. Here, we fabricated the Ti-Al-N multilayer coatings on TC4 substrate by multi-arc ion plating. The corrosion behavior of coating was conducted under the stimulated environment with 20 cycles of salt spray (35 ℃ for 22 h) and hot corrosion (500 ℃ for 2 h). Result showed that the vast majority of corrosive products were accumulated with increasing corrosion cycles, causing the substantial spallation and delamination of coating. However, the unique structures composing of TiAlN columnar crystals and TiN-Ti-TiN equiaxial crystals still benefited the excellent protective performance for coating.

1. Introduction

With the rapid development of light-weight aircrafts and heavy-duty gas turbines, titanium alloys gain the increasingly attention as compressor engine blades, due to the combined characteristics with high specific strength, excellent oxidation resistance and mechanical properties at high temperatures [1–9]. However, these Ti-based mechanical components are apt to be worn by the severe chloride corrosion and stimulated erosion under harsh sandy-marine beyond of 300 °C, which even could lead to the fatal disaster for systems [10]. A coating on the material surface is one of the most feasible protocols as the ample protection, without deterioration of superior properties of substrate simultaneously. To date, various protective coatings with high hardness and good corrosion resistance have been attempted like high-entropy alloy coatings[11,12] ceramic carbide and nitride coatings with special designed microstructures for aerospace sectors [13,14]. Among them, thanks to the high hardness and excellent oxidation resistance [15,16], nitride-based hard coatings such as TiN, ZrN et al. are considered as one of the most promisingly protective candidates to enhance both the mechanical and electrochemical properties of Ti-based substrates, and thereafter greatly improve the life time of titanium components [17–19]. Compared to binary phases, such as TiN, ternary Ti-Al-N coatings have drawn much interests, because of the promising combination with excellent corrosion resistance in NaCl solution and oxidation resistance to 800 °C [20–22].

Current attempts to synthesize Ti-Al-N coatings by physical vapor deposition (PVD) can be mainly categorized to magnetron sputtering and cathodic vacuum arc techniques. It is worthwhile to note that almost Ti-Al-N coatings deposited by these two approaches present the columnar crystalline structure, together with the intrinsic defects of pinholes, voids, micro-cracks and macro-particles [23], which make the coatings more susceptible to be failure in a corrosive environment. In particular, the corrosive chloride and oxygen media could easily penetrate into the coating along the columnar grain boundaries and react directly with the substrate to produce a large number of corrosion products, leading to the substantial failure of the coating or even the substrate [24–26]. One way to solve these issues is to fabricate the multilayer structure rather than single-layer for coatings, in which the growth defects could be suppressed greatly and the corrosive media penetrating to substrate was prevented [27–29]. For example, Li et al. compared the NaCl-induced hot corrosion behavior of single-layer TiN coating and multilayer TiN/Ti coating, where they found the multilayer

* Corresponding authors at: Key Laboratory of Marine Materials and Related Technologies, Zhejiang Key Laboratory of Marine Materials and Protective Technologies, Ningbo Institute of Materials Technology and Engineering, Chinese Academy of Sciences, Ningbo 315201, China.
E-mail addresses: wangzy@nimte.ac.cn (Z. Wang), aywang@nimte.ac.cn (A. Wang).

https://doi.org/10.1016/j.corsci.2023.111431
Received 19 May 2023; Received in revised form 13 July 2023; Accepted 28 July 2023
Available online 29 July 2023

coating performed the excellent corrosion resistance after the salt spray and hot corrosion treatment, respectively [30]. Nevertheless, noted that another significant problem is that the durability of coatings and substrates both show the strong dependence upon the existence form of corrosive medium. As an example, Cao et al. [31] studied the corrosion behavior of Fe-20Cr under NaCl solution spray and solid NaCl deposit in water vapor at 600 ℃, where the former sprayed corrosive medium caused seriously corrosion damage due to the amplified NaCl corrosion by water vapor. In addition, a similar set of conditions were applied to TiN coatings [32], in which the NaCl salt spray and the sprayed solid NaCl particles were firstly conducted at constant temperature, respectively, and then the coatings were subjected to hot corrosion treatment for comparison. It was found that, after the salt spray test, the coatings displayed a more severe hot corrosion with a large area of peeling than those in sprayed solid NaCl particles. As a matter of fact, the coated Ti-based compressors generally serve in the marine environment continuously and cyclically, a typical alternating cycle of corrosions. Specifically, when landing, the coatings undergo the corrosion arisen from ocean atmosphere at room temperature; while operating, the coated components easily suffer from the NaCl-induced hot corrosion. These cycled working conditions for Ti-Al-N coatings scaled up the corrosion damage to a large extent. Unfortunately, the prior knowledge base from mono-cycled salt spray corrosion and hot corrosion is not valuable to the authentic cycled corrosion performance for engine components operating over marine areas. It is preliminarily required to clarify the physical mechanism behind corrosions with periodically alternating salt spray and hot corrosion processes.

In our previous studies, the Ti and TiN layers with various thickness and periodic ratio were designed to improve adhesion-bonding and load-bearing capacity for multi-layer nitride coatings [33,34]. Moreover, the Ti-Al-N layers were alternatively applied to the TiN coatings for the promising purpose of higher oxidation resistance and superior mechanical characteristics [35]. In this work, the same Ti-Al-N multilayer coatings were deposited on titanium alloy (namely Ti-6Al-4V) substrates by a home-made cathodic multi-arc ion plating technology. The corrosion behavior of coatings was conducted by alternating salt spray corrosion at 35 ℃ for 22 h and hot corrosion at 500 ℃ for 2 h with various cycles. The stimulated corrosion failure of coatings were discussed in terms of the structural evolution with synergistic salt spray and hot corrosion. This work provides theoretical support for protective coatings for use in the marine environment and offers a new approach to coating evaluation.

2. Experiments and characterizations

2.1. Coating preparation

The multilayer Ti-Al-N coating was deposited on the Ti-6Al-4V (TC4) alloy substrate using a home-made hybrid deposition system composed of cathodic multi-arc sources and linear ion beam (LIS) source. Specifically, TiAl target (Ti:Al = 67:33) and titanium target (purity of 99.99 %) were applied to multi-arc source for generated metallic plasmas, while LIS source was employed for pre-cleaning process before coating deposition. All TC4 substrates with size of 30 mm (L) × 20 mm(W) × 3 mm (thickness) were firstly sanded and polished to a mirror finish, which were then ultrasonically cleaned in acetone and alcohol for 10 min, respectively. After drying, the cleaned substrates were fixed in the rotated sample holder and put into the deposition chamber. When the chamber was evacuated less than the base pressure of 3×10^{-5} mTorr and the chamber temperature reached to 300 ℃, Ar gas with 33 sccm flow rate was introduced to the LIS source with ion current of 0.2 A for 30 min as etching process, in order to remove the adsorbed contaminants from substrate surface and to improve the coating adhesion. During coating deposition, the buffer-layer of Ti coating was firstly deposited on substrate, and then the transition TiN layer was conducted on Ti layer. Subsequently, two cycles of Ti-Al-N plus controlled TiN-Ti-TiN gradient layer were deposited as multilayer structure, where the designed Ti-Al-N layer acted as the top layer finally. A DC pulsed negative bias of 70 V, 70 V, and 80 V was used for the synthesis of Ti, TiN, Ti-Al-N layer, respectively. Fig. 1 shows the schematic diagram of hybrid deposition system for multilayer coatings. Namely, the Ti buffer layer mainly favored the good bonding strength between coating and TC4 substrate, the TiN transition layer benefited the good mechanical properties of coating together with the strong load-bearing capacity, while the TiAlN functional top-layer contributed the excellent corrosion resistance of the composite coating. Meantime, the inserted TiN-Ti-TiN structure not only acted as the stress absorbed layer to suppress the crack and delamination of coating, but also could hinder the penetrating defects caused during deposition process, further endowing the coating excellent corrosion resistance. The detail deposition information could be referred to our previous work [34].

2.2. Interval corrosion and oxidation test

Since the engine blades faces the corrosive salt atmosphere at harsh marine situation when landing or parking, the simulated salt spray experiment was specially conducted for the Ti-Al-N multilayer coatings. Fig. 2 displays the schematic of stimulated corrosion and oxidation tests alternatively for coatings. Namely, the coating was kept in the salt spray box with a constant temperature at 35 °C and a NaCl concentration at 5 wt% for 22 h spray. Subsequently, hot corrosion tests were performed in a tube furnace connected with atmospheric environment, in which the placed coated samples were firstly heated at 500 °C for 2 h and substantially cooled in air to room temperature (RT). Afterwards, the salt spray process and hot corrosion procedure were repeated alternatively. In other words, one alternating cycle was assigned to the process treated by a RT salt spray for 22 h and hot corrosion stage at 500 °C for 2 h.

2.3. Characterization methods

The crystalline structure and phase formation of the as-prepared coatings and the corroded coatings were investigated by X-ray Diffraction (XRD, Bruker D8 Advance, Germany) with a Cu Kα radiation (λ = 0.154 nm). Surface morphology and cross-sectional microstructures with elemental mapping for coatings were characterized by Scanning Electron Microscope (SEM, FEI Quanta FEG 250) equipped with an Energy Dispersive Spectrometry (EDS, OXFORD X-Max) analyzer. The low-speed saw (IsoMetTM, Buehler, USA) was used to prepare the cross-sectional samples, which were then ultrasonically cleaned with ethanol for 10 min and polished with Leica EM TIX 3X

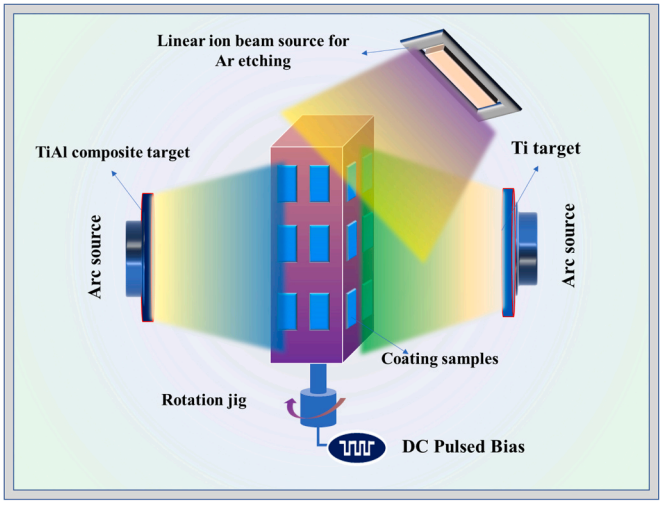

Fig. 1. Schematic diagram of the deposition system for multilayer Ti-Al-N coatings.

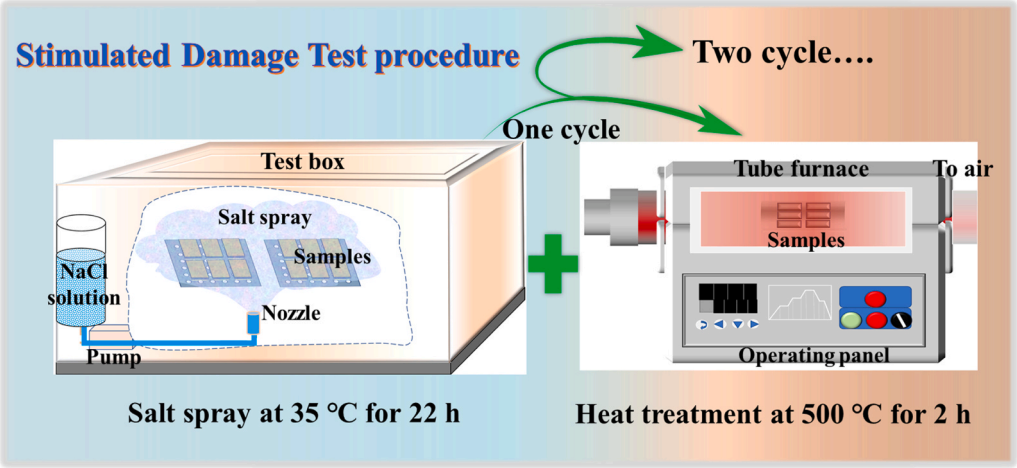

Fig. 2. Schematic of alternative salt spray and hot corrosion test for Ti-Al-N coating.

Wide Ion Beam System (BIB) at a milling voltage of 7 kV. Further detailed microstructure evolution of the coatings were observed by Transmission electron microscopy (TEM, Talos F200x with operating voltage of 200 keV) in the high-angle annular-dark-field (HADDF) analyses. Specimens for TEM test was fabricated by focused ion beam (FIB) lift-out methods using a Zeiss Auriga dual-beam FIB/SEM. The adhesion strength of the coating to the substrate was determined by scratch tests using CSM Revetest (Switzerland) equipped with a diamond Rockwell conical indenter (apex angle of 120° and curvature radius of 200 μm). During the progressive scratch test, the indenter was loaded continuously from 1 N to 100 N and the scratch length, scratch speed was 3.00 mm, 1.00 mm/min, respectively. Each sample was employed at least 3 tests to require accurate results.

3. Results and discussion

3.1. As-deposited Ti-Al-N multilayer coating

Fig. 3a shows the surface morphology and elemental distribution of the as-deposited Ti-Al-N multilayer coating. It was evident that the co-deposited macro-particles and small amount of hole defects could be visible on the coating surface, which might deteriorate the corrosion properties of coating substantially [35]. These defects were mainly ascribed to the instability moving of trigged arc spots during cathodic arc deposition, a well-known phenomenon generating the evaporation of liquid metallic particles together with metallic plasma from cathodic targets [36–38]. Despite of the rich Ti on the formed macro-particles, noted that the element distribution was uniform by EDS results. Fig. 3b illustrates the X-ray diffractograms in the 2θ range from 20° to 90° for the deposited Ti-Al-N multilayer coating. The presented peaks could be assigned to the crystal phases of Ti and TiN, with a dominant (002) and (111) orientation, respectively, while the absence of Al-related phases might be caused by the incorporation or solid-solution of Al atoms in TiN lattice for Ti-Al-N coating [34,39].

Fig. 4 shows the cross-sectional morphology and microstructure of the as-deposited coating by SEM and TEM measurements. As shown in Fig. 4a, the coating presented a uniform thickness of about 13 μm and a clearly periodic multilayered structure. Combined with the element distribution by EDS (Fig. 4b) along growth direction, the coating was composed of the pronounced multilayers including the Ti-Al-N top-layer and the dominated TiN-Ti-TiN sublayer alternatively. Another observation was that the buffer-layer of Ti was strongly bonded with TC4 substrate, indicating the high adhesion strength [34]. Within the gradient TiN-Ti-TiN structure, the element distribution behaved the same gradient characteristics, where the concentration of Ti and N in the position A, B and C varied in range of 61.40 ± 0.5, 69.22 ± 0.7, 56.57 ± 1.0 at% and 38.60 ± 0.4, 30.78 ± 0.8, 43.43 ± 1.1 at%, respectively. The TEM characterization was used further to address the cross-sectional microstructure of as-deposited coating. As shown in Fig. 4d, a dense multilayer structure with dominated columnar feature was obtained for coatings. Furthermore, the selected area electron diffraction (SAED) patterns shown in I and II demonstrated that these columnar crystals could be assigned to the layer with (200)-oriented TiN and (101)-oriented Ti phases, the other layer shows an isometric growth

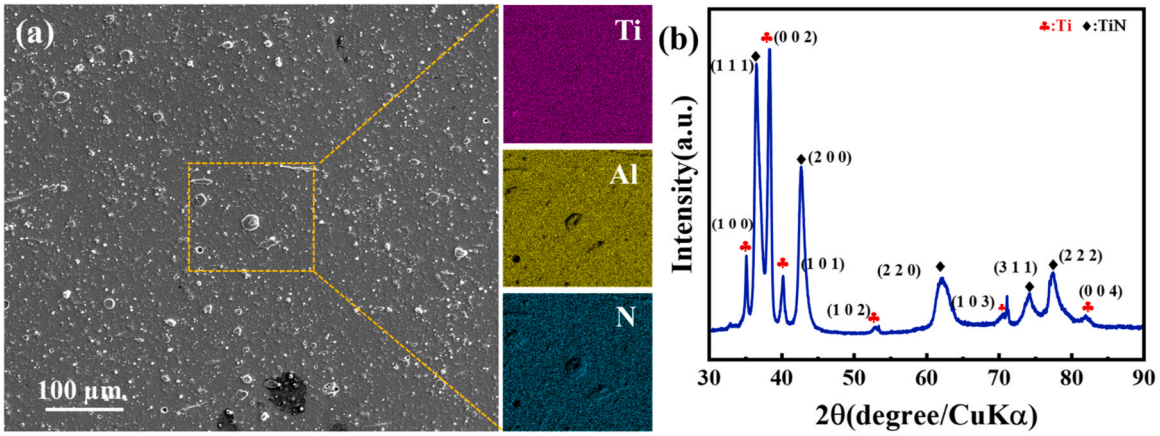

Fig. 3. (a) Surface morphology and corresponding EDS element mappings and (b) XRD diffractograms of the as-deposited Ti-Al-N multilayer coating.

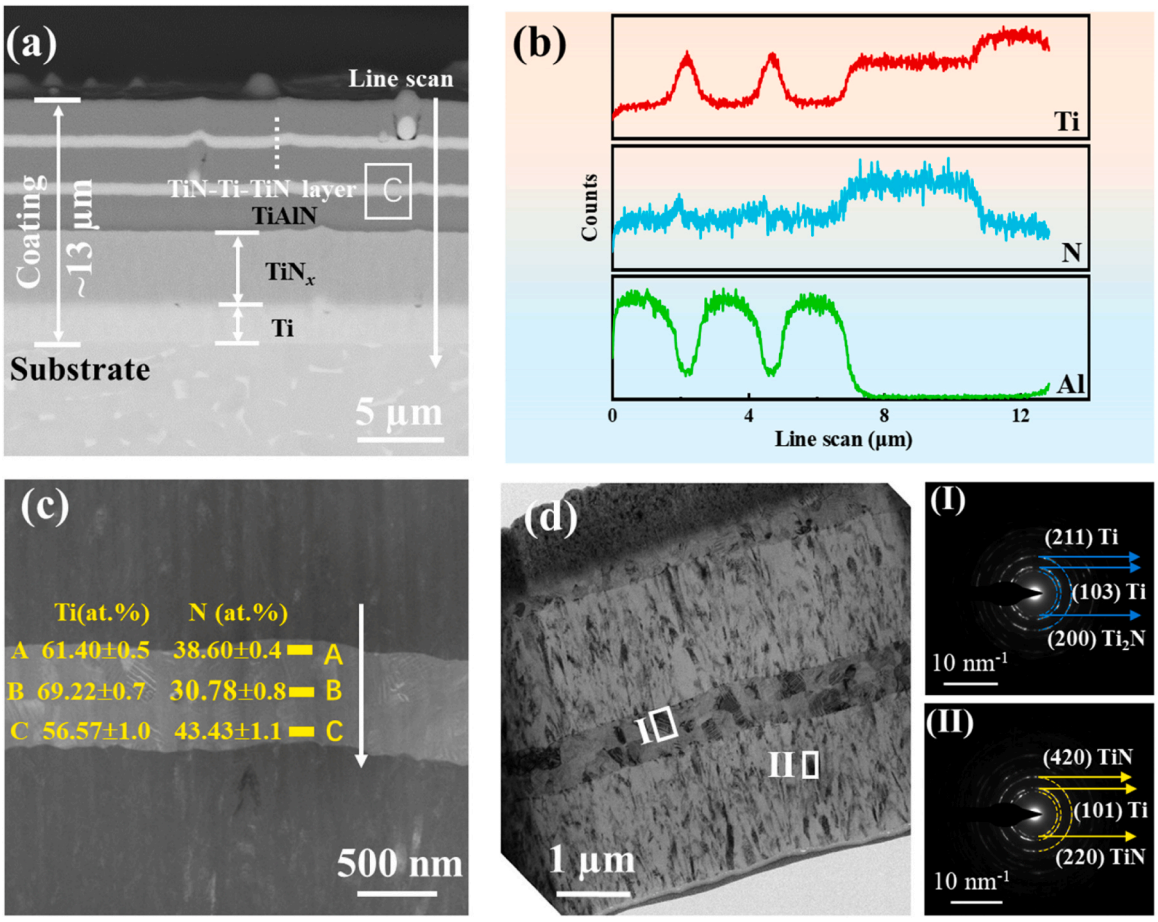

Fig. 4. (a) Cross-sectional SEM micrographs and (b) corresponding line-scanning results of Ti (red), Al (green), N (cyan) along the marked white arrow in a; (c) Point-scanning TEM micrographs of the TiN-Ti-TiN sublayer; (d) Selected area electron diffraction patterns: (I) and (II) SAED of the Ti-Al-N layer and TiN-Ti-TiN layer.

of (200)-oriented Ti_2N and a large number of Ti crystalline phases similar to those previously reported in the literature [40]. Compared to traditional mono-layer coating with coarse columnar structure, the alternating multilayer structure composing of columnar crystals and equiaxed crystals provide the strong ability to suppress the direct penetration of corrosive media from coating into substrate, resulting in the excellent corrosion resistance [39].

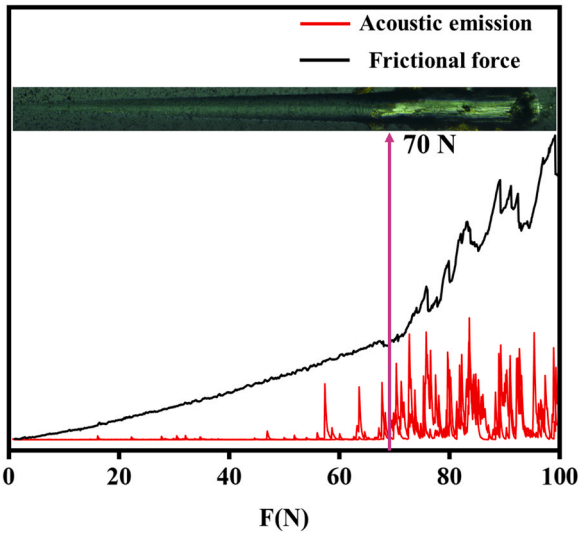

Fig. 5. The strong adhesion strength of the Ti-Al-N multilayered coatings on TC4 substrates.

Fig. 5 shows the adhesion strength of the multilayered coating obtained by the scratch tester with a progressive load. Once the load force reached to 70 N, a distinct increase was found from the acoustic signal. Taking the combinational in-situ scratch morphology, the coating obviously peeled off from the substrate with the exposure of pristine substrate at 70 N. Therefore, it could be identified that the coating displayed a high adhesion strength about 70 N on the TC4 substrate.

3.2. Ti-Al-N multilayer coatings after stimulated corrosion and oxidation test

Fig. 6 presents XRD patterns of the deposited Ti-Al-N multilayer coatings after different corrosion cycles test. The results showed that the phases including NaCl, TiO_2 and $Na_4Ti_5O_{12}$ appeared in the spectra after one corrosion cycle, which was consistent with other reports [35,41,42]. In general, TiO_2 was generated from the coating oxidation during the hot corrosion process, as elucidated from Eqs. (1)–(2). Furthermore, TiO_2 would subsequently react with oxygen and NaCl salt, which enabled the formation of Na_2TiO_3 and $Na_4Ti_5O_{12}$ phases, like the reactions in Eqs. (3)–(4). Beyond of these products, no other corrosion phases were observed in the whole corrosion process. Further increasing the corrosion cycles to 10, the new dominated phases of Ti_2N crystalline was detected from the inner layer of multilayer coating, due to the promoted loose structure by corrosion. However, after 20 corrosion cycles the XRD results were still dominated by the main phases of the coating, TiN and Ti_2N. Despite the generated corrosion products during test, the coating demonstrated the superior corrosion resistance in the harsh environment of alternated salt spray and hot corrosion with 20 cycles, which

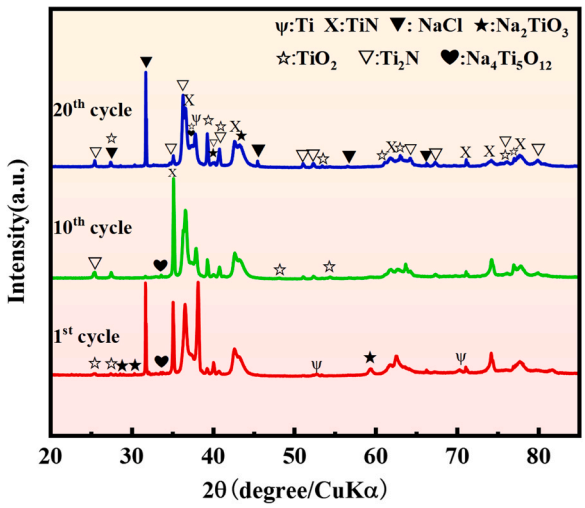

Fig. 6. XRD patterns of the Ti-Al-N multilayer coatings after different corrosion cycles.

could be attributed to the unique multilayer structure and intrinsic corrosion resistance in Ti-Al-N coatings to a great extent [34].

$$2TiN(s) + 2O_2(g) \rightarrow 2TiO_2(s) + N_2(g) \quad (1)$$

$$Ti + O_2(g) \rightarrow 2TiO_2(s) \quad (2)$$

$$4NaCl(s) + O_2(g) + 2TiO_2(s) \rightarrow 2Na_2TiO_3(s) + 2Cl_2(g) \quad (3)$$

$$4NaCl(s) + O_2(g) + 5TiO_2(s) \rightarrow Na_4Ti_5O_{12}(s) + 2Cl_2(g) \quad (4)$$

To further characterize the structural evolution related to corrosion behavior, Fig. 7 shows the surface morphologies of Ti-Al-N multilayer coating after different corrosion cycles. For 1st cycled sample, obvious cracks together with the formed oxides were visible near the crystalline salt (Fig. 7a), indicating corrosion damage to the coating. Since the corrosion media could quickly penetrate to the coating along the growth defects and corrosion failure areas, quite a few new corrosion products, cracks and small pieces of delaminated chips emerged in the original peeling area after 10 cycled corrosion tests (Fig. 7b), which led to the severe peeling and spallation of coating than those in 1st cycled case. Further increasing the corrosion cycles to 20 caused the worst peeling phenomena and spallation failure in the coating surface (Fig. 7c). Moreover, some corrosion pits were obtained in the local peeling area on the exposed coating surface, that could be arisen from accumulated corrosion products in the coating.

Fig. 8 shows the surface morphology and related EDS elements distribution of the Ti-Al-N multilayer coating with various corrosion cycles. For the 1st corrosion cycled sample, the evident microcracks were observed near the macroparticles and the accumulated products emerged in the coating surface, as shown in Fig. 8a. According to the EDS mapping results, these corroded products were enriched with O and Ti, implying the consistently formed TiO_2 phases in Fig. 6. After the 10th corrosion cycle test, the spallation area was appeared in the coating surface, which could be the result of accelerated corrosion products and the peeling off from coating during stimulated corrosions (Fig. 8b). Similarly, the O and Ti were also enriched and Al composition was deficiency in the damage area, as shown in the corresponding EDS mapping. Once the corrosion cycles reached to 20 , the more larger peeling areas were achieved in the coating surface (Fig. 8c). In addition, the new peeling occurred in the previous peeling regions, due to the delamination of outer layer for coating and substantially disabled protective effect. In this case, the corrosive media directly passed through the coating inside, which finally resulted in the spallation of coating. Combining with the results of EDS in Fig. 8, it could be concluded that the corrosion damage was firstly formed at the growth defect of coating surface, and the sprayed crystalline salt played the key role in accelerating the corrosive failure of the coating under the synergistic effect of alternated salt spray and hot corrosion processes.

In order to elucidate the elemental distribution during the corrosion cycles, Fig. 9 displayed the selected surface morphologies for three different tests, representatively, where the compositions of Ti, Al, N and

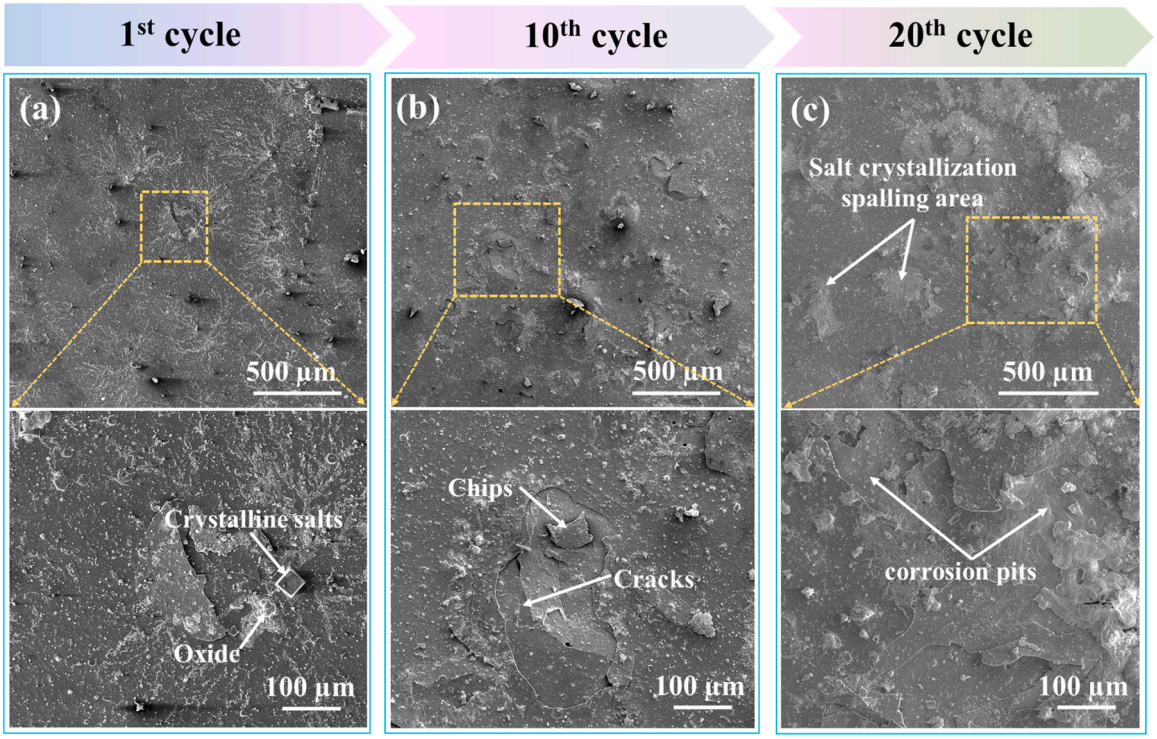

Fig. 7. Surface morphology of the Ti-Al-N multilayer coating after different corrosion cycles: (a) 1st cycle; (b) 10th cycle; (c) 20th cycle.

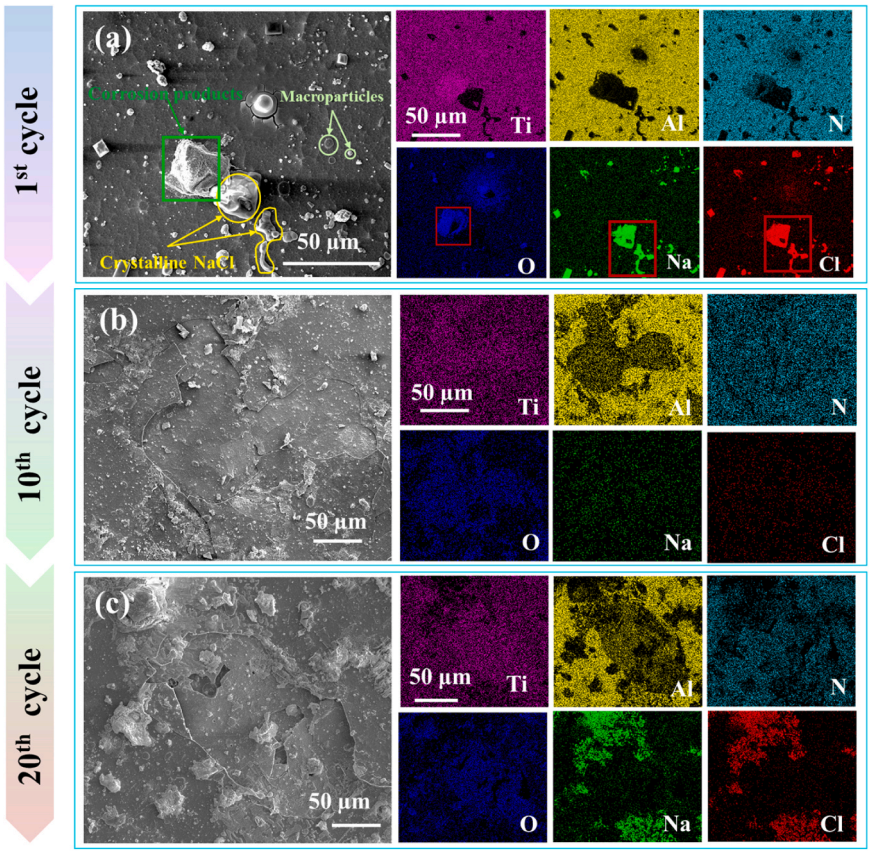

Fig. 8. Surface morphology and related elements distribution of the Ti-Al-N multilayer coating with various corrosion cycles: (a) 1st cycle; (b) 10th cycle; (c) 20th cycle.

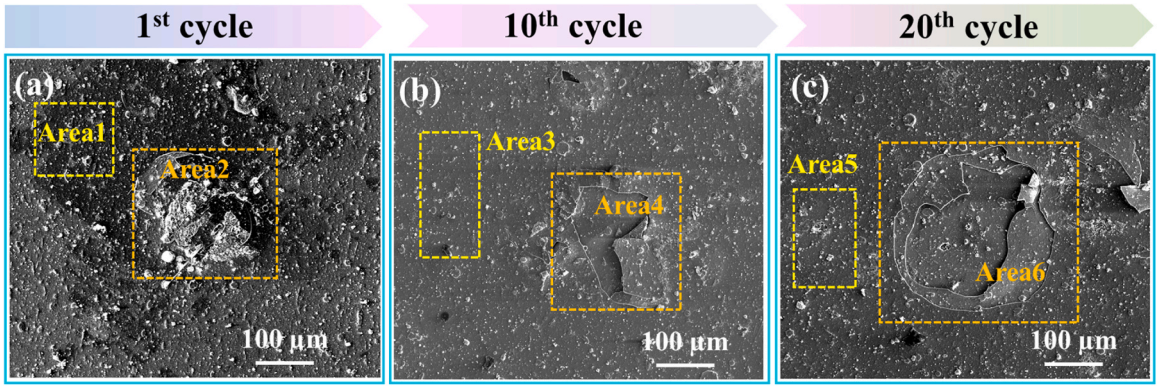

Fig. 9. The representative SEM morphology with different corrosion cycles: (a) 1st cycle, (b) 10th cycle, (c) 20th cycle.

O in the detected regions of coating were listed in Table 1. For all peeling and spallation regions, the oxygen content increased gradually with increase of corrosion cycles, indicating the more and more serious corrosion damage. On the other side, the downward tendency was visible for N content, especially evident in the peeling areas of position 2, 4 and 6. The reason might be attributed to the reaction between TiN and O, where the N_2 was generated and overflowed subsequently [30,32,39], as indicated in Eq. (1). Similar decreasing trend in content of Al element was illustrated in the peeling areas of 2, 4 and 6, which was correlated to the peeling of the outermost Ti-Al-N coating. Different with the peeling regions, however, noted that both the content of Al and Ti in unpeeling areas (position 1, 3, 5) almost remained constant regardless of the corrosion cycles. In general, the increase in oxygen content replied the formation and accumulation of corrosive oxides, while the release of N_2 gas occurred from the reaction of TiN and O. These was the dominated reason for the peeling damage of the coating. Beyond of the

Table 1
Chemical composition of the points in Fig. 8 (Areas 1, 3, 5 represent the non-peeling, and Areas 2, 4, 6 display the spallation region).

Point position	Elemental content (at%)			
	O	N	Al	Ti
Area 1	6.60 ± 1.0	37.01 ± 0.8	34.70 ± 1.1	21.37 ± 1.2
Area 2	17.67 ± 1.1	28.35 ± 0.5	31.91 ± 0.4	22.70 ± 0.8
Area 3	11.18 ± 0.7	33.28 ± 0.6	33.91 ± 1.2	21.39 ± 0.9
Area 4	23.26 ± 0.9	24.85 ± 0.3	28.57 ± 0.7	23.07 ± 0.4
Area 5	18.56 ± 0.6	28.45 ± 0.3	32.14 ± 1.1	20.31 ± 0.7
Area 6	31.06 ± 0.5	19.11 ± 0.8	25.80 ± 1.5	23.38 ± 1.3

peeling effect, moreover, the N element content in the peeling area decreased dramatically compared with that in the unpeeling region, which could be ascribed to the accelerated corrosion reaction of the corrosively galvanic cell formed by the soft-hard multilayer interfaces.

Fig. 10 shows the cross-sectional microstructure of the coating after different corrosion cycles test. It was clear that, under the 1st corrosion cycle, all the coating was strongly adhered to the substrate with the dense multilayered interfaces, despite of the slight corrosion appeared in the outmost surface (Fig. 10a). However, once the corrosion cycles reached to 10 (Fig. 10b), the corrosion media easily penetrated into the coating interfaces along the inherent defects including macro-particles and pinholes[35]. As a result, the serious isolation between interfaces and the delamination with cracks were obtained in the coating. Interestingly, noted that the peeling failure only occurred along the interface within multilayered structure rather than perpendicular to the growth direction of coating, indicating the maintained corrosion resistance of coated substrate. Further increasing the corrosion cycles to 20 led to the worst stratification within the periodic multilayered structure and small part of spallation of the coating, which was assigned to the slight decreases of protective capability (Fig. 10c).

Moreover, the EDS mapping images of selected region in Fig. 10c illustrated that a significant oxide layer appears at the surface of the coating and at the multilayer interface, but there is no enrichment of corrosion media within the TiAlN layer, as shown in Fig. 10d. It could be thus deduced that the corrosive galvanic cell was generated between the multilayer interfaces of the coating. Furthermore, the EDS mapping results also show that no obvious enrichment of corrosion medium was found within the inside Ti-Al-N layer closer to the substrate. In this case, the achievement of excellent salt-coupled hot corrosion resistance remained in the multilayered Ti-Al-N coatings were mainly attributed to the two factors. One is the outward TiAlN layer displayed the quite high stability after harsh alternated salt spray and hot corrosion cycles. Another reason could be benefited from the strong adhesion among coatings layers and coating/TC4 substrate [34].

To complement the microstructural evolution of the coating with various corrosion cycles tests, Fig. 11 shows the TEM cross-sectional morphologies of the non-peeling area in coating after 20 corrosion cycles. Obviously, the coating maintained a dense multi-layered TiAlN structure in outmost layer without any peeling or laminar delamination (Fig. 11a), where the thickness of inserted TiN-Ti-TiN gradient layer was about 559.65 nm. In addition, an oxide layer enriched with Ti, Al, O and Na was formed in the coating surface, while the infiltration of corrosive media composed of O, Na and Cl was absent from the inside of coating (Fig. 11b). This identified the excellent salt spray coupled hot corrosion resistance of the coating. Based on the HAADF image of representative area c in Fig. 11a, the thickness of generated oxide layer was about 45.19 nm on the outmost TiAlN layer, even presenting a loose structure with a large amount of hole defects. Combined with the XRD and above-mentioned reaction analysis, these defects could mainly be ascribed to the formation of gaseous corrosive products during synergistic salt-hot corrosion process. According to the HRTEM image shown in Fig. 11d, the encountered corrosion products of oxide layer were composed of $Na_4Ti_5O_{12}$ and TiO_2. Moreover, Fig. 11d identified that the lattice fringes with an interplanar spacing of 1.974 Å and 1.868 Å was assigned to the (311) plane of $Na_4Ti_5O_{12}$ and the (200) plane of TiO_2, respectively.

For comparison, Fig. 12 illustrates the TEM cross-sectional characterization of the peeling area after 20 corrosion cycles. Distinct difference could be found in the region of peeling surface, where the formed oxide layer next to the TiN-Ti-TiN sublayer was mainly composed of Na, Ti, and O, as shown in Fig. 12a and Fig. 12b. In addition, the HAADF image in Fig. 12c indicated that the oxide layer with thickness of 152.1 nm presented the loose and porous structure with massive cracks. During the substantial increase of corrosion cycles, these porous structures of the oxide layer would significantly deteriorate the protective capability of next Ti-Al-N layer, causing the slight peeling off of oxide products from the coatings. Nevertheless, the important observation was that the corrosive galvanic cell was promoted within the coating interface due to the accelerated corrosion reaction. This in turn benefited the increase in thickness of oxide layer was around 152.1 nm, almost more than three times thicker than that in the unpeeled area (45.19 nm), as shown in Fig. 12c. And the HRTEM bright-field image revealed the

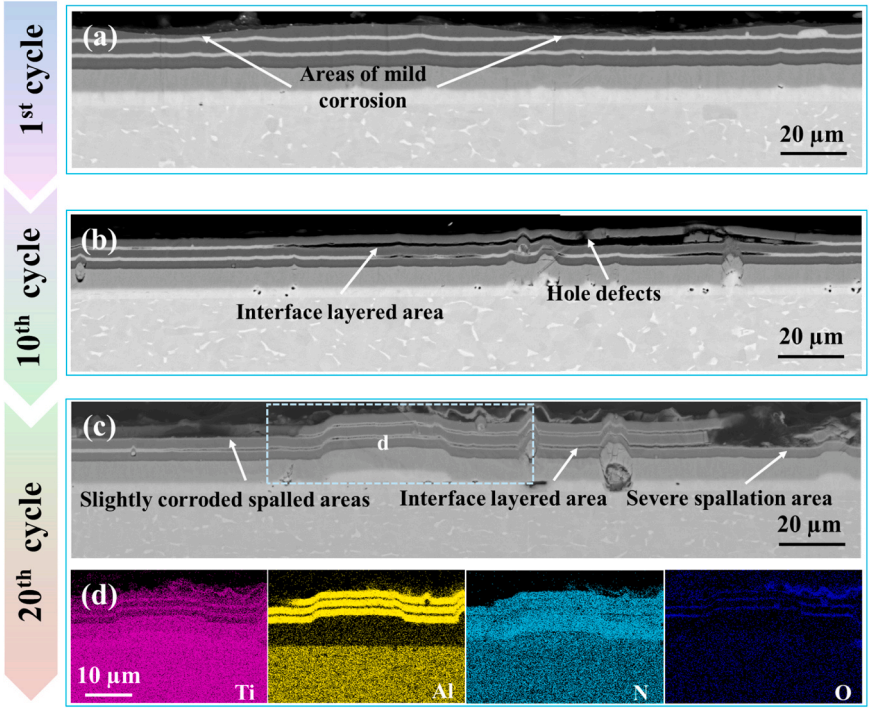

Fig. 10. The cross-section morphology of Ti-Al-N multilayer coating after different corrosion cycles: (a) 1st cycle, (b) 10th cycle, (c) 20th cycle, (d) Corresponding EDS mapping of the selected area d.

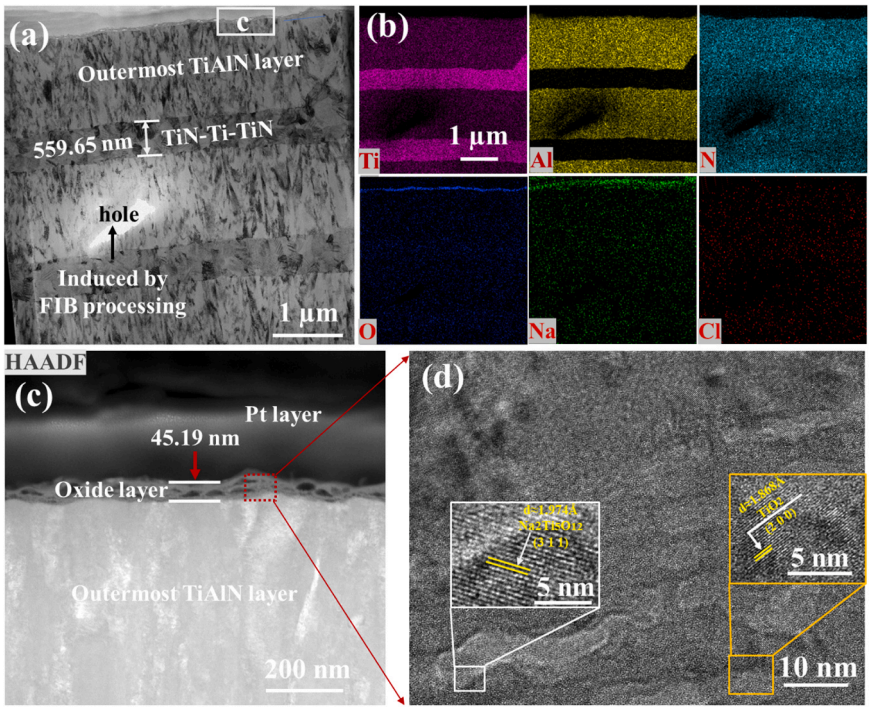

Fig. 11. Cross-sectional morphologies of non-peeling area in coating after twenty corrosion cycles: (a) STEM image and (b) corresponding EDS mapping, (c) HAADF image of the area c in (a), (d) HRTEM bright-field image of the corrosion area d in (c).

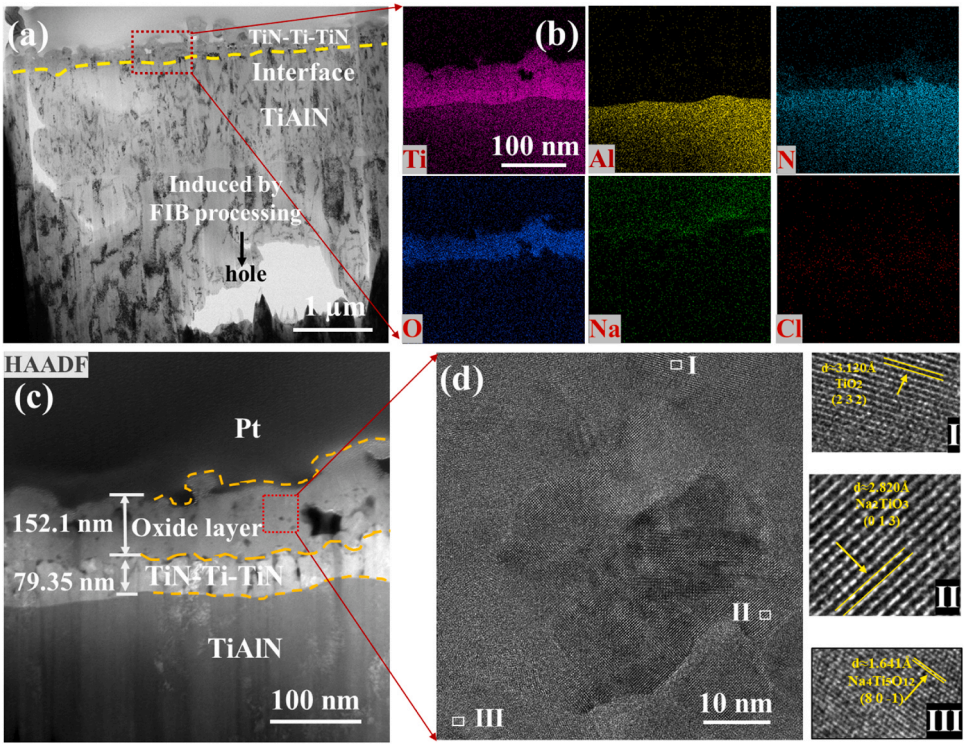

Fig. 12. Cross-sectional views of peeling area after twenty corrosion cycles. (a) STEM image of the peeling area; (b) Corresponding EDS mapping of area b; (c)–(d) HAADF image of area c and HRTEM bright-field image of the selected corrosion area.

lattice fringes with an interplanar spacing of 3.120 Å (region I), 2.820 Å (region II) and 1.653 Å (region III), which was corresponded to the (232) plane of TiO_2, (013) plane of Na_2TiO_3, and (80−1) plane of $Na_4Ti_5O_{12}$, respectively. As a summary, the loose and porous structure dominated by titanate corrosion products was most likely consisting of Na_2TiO_3 and $Na_4Ti_5O_{12}$, which accelerated the sub-layers adhesion and the peeling failure of coating.

Lastly, to clarify the versatility of the multilayer Ti-Al-N coatings with various salt-coupled hot corrosion cycles, Fig. 13 illustrates the schematic diagram of the corrosive damage mechanism in terms of the

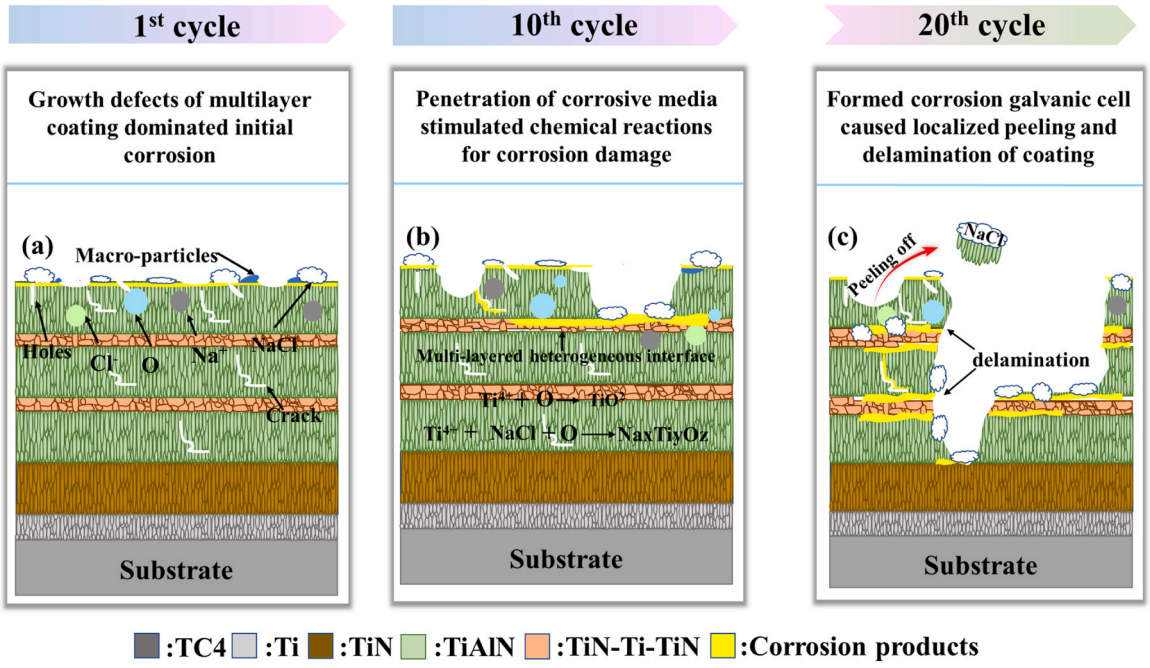

Fig. 13. Schematic diagram of the corrosion mechanism for Ti-Al-N multilayer coating in salt spray (22 h) coupled hot corrosion (2 h) for different cycles alternately.

structural evolution. For the initial stage of the synergistic corrosion test (Fig. 13a), the damage of coating occurred firstly in the defective regions with co-deposited macro-particles and pinholes during the growth of coating. During the salt spray process, NaCl solution passed through the coating along the corrosion channels yielded by these defects, companying with the formation of large number of crystal salts in the defect area. With the following hot corrosion process, the oxygen element could easily accumulate around the crystalline salts, and thereafter reacted with TiN to generate TiO_2 phases and gaseous N_2, or alternatively reacted with Ti to produce TiO_2 phases (Eqs. (1)–(2)). Next, part of TiO_2 products reacting with the NaCl and O led to the appearance of $Na_4Ti_5O_{12}$ and Cl_2 (Eq. (3)), meanwhile the Cl_2 consumed TiN to form $TiCl_4$ and N_2 (Eq. (4)). This process could continuously accelerate the corrosion failure of the coating. In particular, noted that the gaseous formation including N_2 and Cl_2 was another key factor to stimulate the corrosion damage with serious accumulation of the porous corrosion products.

As the corrosion cycle increased to 10 (Fig. 13b), Na_2TiO_3 as corrosion product was also promoted despite of $Na_4Ti_5O_{12}$. The reaction could be identified in Eq. (5). Due to the vast accumulation of corrosion products in $Na_xTi_yO_z$, the bonding strength within multilayer in coating was reduced dramatically, which finally induced the localized peeling off. Meanwhile, the existence of Ti_2N phases in the TiN-Ti-TiN sublayer would also gradually reacted with the corrosive medium that entered the interfaces, and favored the more production of TiO_2 further (Eq. (6)).

Table 2
Standard Gibbs free energy changes of reactions with respect to Ti-Al-N multilayer coating at 500 ℃ [32,38,43].

Eq.	Chemical reaction	$\Delta G°_{773\ K}$ (kJ mol^{-1})
(1)	$2TiN(s) + 2O_2(g) \rightarrow 2TiO_2(s) + N_2(g)$	-420.39
(2)	$2Ti\ (s) + O_2(g) \rightarrow TiO_2(s)$	-654.17
(3)	$4NaCl(s) + O_2(g) + 5TiO_2(s) \rightarrow Na_4Ti_5O_{12}(s) + 2Cl_2(g)$	-161.67
(4)	$2TiN(s) + 4Cl_2(g) \rightarrow 2TiCl_4(g) + N_2(g)$	-372.84
(5)	$4NaCl(s) + O_2(g) + 2TiO_2(s) \rightarrow 2Na_2TiO_3(s) + 2Cl_2(g)$	-62.94
(6)	$2Ti_2N\ (s) + 4O_2(g) \rightarrow 4TiO_2(s) + N_2(g)$	-99.37

Moreover, for all these discussions, the negative Gibbs free energy of the above-formulated reactions (Table 2) enabled the possibility in hot corrosion environment with the thermodynamic aspect. In parallel, another important issue was that the corrosive medium entered easily to the interior of the coating along both the growth defect and peeling zone, generating a corrosive galvanic cell at the multi-layer interfaces. Thereafter, the tremendous corrosion products were evolved and continuously deteriorated the bonding performance between interfaces which interpreted the aggravation of corrosive failure and spallation of the coating.

An even more critical phenomena shown in Fig. 13c was that, with the increase of corrosion cycles to 20, the vast majority of corrosion products were accumulated in the outmost surface and intrinsic interface of the coating. In addition, salt and oxygen become more and more enriched during the synergistic corrosion test, the corrosive reactions were intensively stimulated. All these conductors led to the continuous interfacial damage and large area spallation of the coating along the interface. More surprising expected results were that the coating spallation would be intensified, and the crystalline salts adhered to the outmost layer were flaked off. This resulted in the continuous damage of coating with loose structure, which in turn provided the further penetration of corrosion medium through these delamination regions, a fact leading support to the explanation for the accelerated failure of the multilayer Ti-Al-N coating.

4. Conclusion

The Ti-Al-N multilayer coating composed of TiN-Ti-TiN gradient layer and outmost TiAlN layer was fabricated on the titanium alloy (TC4) substrate by a home-made cathodic multi-arc ion plating technology. The dependence of corrosion behavior of Ti-Al-N multilayered coating was focused as a function of the conducted synergistic corrosion test, where the periodical corrosion cycle process including one stage of salt spray corrosion at room temperature and another stage of hot corrosion at 500 °C were controlled with namely 1, 10 and 20 cycles, respectively. The corrosion failure was discussed in terms of the microstructural evolution and the correlated reactions with formed corrosion products were proposed for the understanding of accelerated corrosion mechanism. The results indicated that the corrosion phases

including NaCl, TiO_2 and $Na_4Ti_5O_{12}$ emerged firstly after one corrosion cycle, and the extra TiN, Ti_2N crystalline phases were detected substantially with the increase of corrosion cycles up to 20. The formation of N_2 and Cl_2 gaseous were proposed to play key role in the accelerated corrosion damage, where the vast majority of accumulated porous products were achieved with increasing the salt-coupled hot corrosion cycles. Another observation of the corrosion products could be identified by the Ti oxides and the related titanate composites, including $Na_4Ti_5O_{12}$ and Na_2TiO_3. Due to the generation of corrosion products in early stage, the further peeling off was triggered by the galvanic corrosion cell occurred in the multilayer interfaces, which enabled the easy penetration of corrosive chloride media to the intrinsic layer of coating. Finally, the spallation and delamination of the localized region were induced for the deterioration of the multilayer Ti-Al-N coatings. Neverthless, the most important result was that even the coatings suffered from the stimulated corrosion damage, the remained manifest of the excellent salt-coupled hot corrosion resistance was surprisingly obtained in the Ti-Al-N multilayer coatings, which was probability attributed to the excellent salt-hot corrosion resistance of the TiAlN layer and the benefits of strong bonded strength between coating and substrate, as well as the specially alternated periodic structures composing of TiAlN columnar crystals and TiN-Ti-TiN equiaxial crystals.

CRediT authorship contribution statement

Dingwei Zhou: Methodology, Investigation, Data curation, Writing – original draft. **Zhenyu Wang:** Conceptualization, Validation, Writing – review & editing. **Yan Zhang:** Resources, Visualization, Data curation. **Jingjun Yan:** Formal analysis, Investigation. **Guanshui Ma:** Validation, Investigation. **Xiaojun Hu:** Formal analysis, Writing – review & editing, Supervision. **Peiling Ke:** Writing – review & editing, Supervision. **Aiying Wang:** Project administration, Writing – review & editing, Supervision.

Declaration of Competing Interest

The authors declare that they have no known competing financial interests or personal relationships that could have appeared to influence the work reported in this paper.

Data Availability

No data was used for the research described in the article.

Acknowledgements

This work was financially supported by the National Science Found for Distinguished Young Scholars of China (52025014), the National Natural Science Foundation of China (52171090, 52101109), the Youth Innovation Promotion Association CAS (2023312), and Science and Technology Innovation 2025 Major Project of Ningbo (2022Z011).

References

[1] M.R. Geng, G.Y. He, Z.P. Sun, J. Chen, Z.F. Yang, Y.Q. Li, Corrosion damage mechanism of TiN/ZrN nanoscale multilayer anti-erosion coating, Coatings 8 (2018) 400.
[2] F. Yang, B. Gabbitas, Feasibility of producing Ti-6Al-4V alloy for engineering application by powder compact extrusion of blended elemental powder mixtures, J. Alloy. Compd. 695 (2017) 1455–1461.
[3] M.S.I. Chowdhury, S. Chowdhury, K. Yamamoto, B.D. Beake, B. Bose, A. Elfizy, D. Cavelli, G. Dosbaeva, M. Aramesh, G.S. Fox-Rabinovich, S.C. Veldhuis, Wear behaviour of coated carbide tools during machining of Ti6Al4V aerospace alloy associated with strong built up edge formation, Surf. Coat. Technol. 313 (2017) 319–327.
[4] G. Lütjering, Influence of processing on microstructure and mechanical properties of (α + β) titanium alloys, Mater. Sci. Eng.: A 243 (1998) 32–45.
[5] A. Carman, L.C. Zhang, O.M. Ivasishin, D.G. Savvakin, M. Matviychuk, E. V. Pereloma, Role of alloying elements in microstructure evolution and alloying elements behaviour during sintering of a near-β titanium alloy, Mater. Sci. Eng.: A 528 (2011) 1686–1693.
[6] M. Hagiwara, S. Emura, Blended elemental P/M synthesis and property evaluation of Ti-1100 alloy, Mater. Sci. Eng.: A 352 (2003) 85–92.
[7] W.J. Evans, Optimising mechanical properties in alpha + beta titanium alloys, Mater. Sci. Eng.: A 243 (1998) 89–96.
[8] R.R. Boyer, An overview on the use of titanium in the aerospace industry, Mater. Sci. Eng.: A 213 (1996) 103–114.
[9] D. Banerjee, J.C. Williams, Perspectives on titanium science and technology, Acta Mater. 61 (2013) 844–879.
[10] D.P. Zhou, H. Peng, L. Zhu, H.B. Guo, S.K. Gong, Microstructure, hardness and corrosion behaviour of Ti/TiN multilayer coatings produced by plasma activated EB-PVD, Surf. Coat. Technol. 258 (2014) 102–107.
[11] Y. Fu, C. Huang, C.W. Du, J. Li, C.D. Dai, H. Luo, Z.Y. Liu, X.G. Li, Evolution in microstructure, wear, corrosion, and tribocorrosion behavior of Mo-containing high-entropy alloy coatings fabricated by laser cladding, Corros. Sci. 191 (2021), 109727.
[12] H.X. Cheng, Z.M. Pan, Y. Fu, X.F. Wang, Y. Wei, H. Luo, X.G. Li, Review—corrosion-resistant high-entropy alloy coatings: a review, J. Electrochem. Soc. 168 (2021), 111502.
[13] J.C. Oliveira, A. Cavaleiro, C.M.A. Brett, Influence of sputtering conditions on corrosion of sputtered W-Ti-N thin film hard coatings: salt spray tests and image analysis, Corros. Sci. 42 (2000) 1881–1895.
[14] G.Z. Xie, X.Y. Lin, K.Y. Wang, X.Y. Mo, D.J. Zhang, P.H. Lin, Corrosion characteristics of plasma-sprayed Ni-coated WC coatings comparison with different post-treatment, Corros. Sci. 49 (2007) 662–671.
[15] I. Gurrappa, A.K. Gogia, Development of oxidation resistant coatings for titanium alloys, Mater. Sci. Technol. 17 (2001) 581–587.
[16] F. Weng, C.Z. Chen, H.J. Yu, Research status of laser cladding on titanium and its alloys: a review, Mater. Des. 58 (2014) 412–425.
[17] V.R. Parameswaran, J.P. Immarigeon, D. Nagy, Titanium nitride coating for aero engine compressor gas path components, Surf. Coat. Technol. 52 (1992) 251–260.
[18] M. Pepi, R. Squillacioti, L. Pfledderer, A. Phelps, Solid particle erosion testing of helicopter rotor blade materials, J. Fail. Anal. Prev. 12 (2012) 96–108.
[19] M.W. Reedy, T.J. Eden, J.K. Potter, D.E. Wolfe, Erosion performance and characterization of nanolayer (Ti, Cr) N hard coatings for gas turbine engine compressor blade applications, Surf. Coat. Technol. 206 (2011) 464–472.
[20] A.A. Matei, I. Pencea, M. Branzei, D.E. Trancă, G. Ţepeş, C.E. Sfăt, E. Ciovica, A. I. Gherghilescu, G.A. Stanciu, Corrosion resistance appraisal of TiN, TiCN and TiAlN coatings deposited by CAE-PVD method on WC-Co cutting tools exposed to artificial sea water, Appl. Surf. Sci. 358 (2015) 572–578.
[21] X. Cao, W.S. Xu, W.F. He, A method for evaluating the impact wear behavior of multilayer TiN/Ti coating, Coatings 10 (2020) 132.
[22] Z.P. Sun, G.Y. He, Q.J. Meng, Y.Q. Li, X.D. Tian, Corrosion mechanism investigation of TiN/Ti coating and TC4 alloy for aircraft compressor application, Chin. J. Aeronaut. 33 (2020) 1824–1835.
[23] H. Curtins, PLATIT: a new industrial approach to cathodic arc coating technology, Surf. Coat. Technol. 76–77 (1995) 632–639.
[24] Z.Y. Wang, X.W. Li, W.T. Li, P.L. Ke, A.Y. Wang, Comparative study on oxidation behavior of Ti_2AlN coatings in air and pure steam, Ceram. Int. 45 (2019) 9260–9270.
[25] J.Y. Chen, G.P. Yu, J.H. Huang, Corrosion behavior and adhesion of ion-plated TiN films on AISI 304 steel, Mater. Chem. Phys. 65 (2000) 310–315.
[26] E. Bemporad, M. Sebastiani, C. Pecchio, S.D. Rossi, High thickness Ti/TiN multilayer thin coatings for wear resistant applications, Surf. Coat. Technol. 201 (2006) 2155–2165.
[27] C. Liu, A. Leyland, Q. Bi, A. Matthews, Corrosion resistance of multi-layered plasma-assisted physical vapour deposition TiN and CrN coatings, Surf. Coat. Technol. 141 (2001) 164–173.
[28] E. Alat, A.T. Motta, R.J. Comstock, J.M. Partezana, D.E. Wolfe, Multilayer (TiN, TiAlN) ceramic coatings for nuclear fuel cladding, J. Nucl. Mater. 478 (2016) 236–244.
[29] H.Z. Guo, Q.Q. Sun, D.P. Zhou, Y. Miao, Y.X. Wang, Q. Wang, X.J. Li, Erosion behavior of CrN, CrAlN and CrAlN/CrN multilayer coatings deposited on Ti6Al4V, Surf. Coat. Technol. 437 (2022), 128284.
[30] R.Z. Li, S.H. Wang, J.B. Pu, D.P. Zhou, M. Yu, Y. Wei, W.M. Guo, Study of NaCl-induced hot-corrosion behavior of TiN single-layer and TiN/Ti multilayer coatings at 500 ℃, Corros. Sci. 192 (2021), 109838.
[31] M. Cao, L. Liu, Z.F. Yu, L. Fan, Y. Li, F.H. Wang, Studies on the corrosion behavior of Fe-20Cr alloy in NaCl solution spray at 600 ℃, Corros. Sci. 133 (2018) 165–177.
[32] R.Z. Li, S.H. Wang, D.P. Zhou, J.B. Pu, M. Yu, W.M. Guo, A new insight into the NaCl-induced hot corrosion mechanism of TiN coatings at 500 °C, Corros. Sci. 174 (2020), 108794.
[33] J.T. Shuai, X. Zuo, Z.Y. Wang, L.L. Sun, R.D. Chen, L. Wang, A.Y. Wang, P.L. Ke, Erosion behavior and failure mechanism of Ti/TiAlN multilayer coatings eroded by silica sand and glass beads, J. Mater. Sci. Technol. 80 (2021) 179–190.
[34] H.T. Ruan, Z.Y. Wang, L. Wang, L.L. Sun, H. Peng, P.L. Ke, A.Y. Wang, Designed Ti/TiN sub-layers suppressing the crack and erosion of TiAlN coatings, Surf. Coat. Technol. 438 (2022), 128419.
[35] C.J. Feng, M.S. Li, L. Xin, S.L. Zhu, F.H. Wang, Mechanical properties and oxidation behavior of a graded (Ti,Al)N coating deposited by arc-ion plating, Oxid. Met. 65 (2006) 307–327.
[36] N.M. Lin, X.B. Huang, X.Y. Zhang, A. Fan, L. Qin, B. Tang, In vitro assessments on bacterial adhesion and corrosion performance of TiN coating on Ti6Al4V titanium alloy synthesized by multi-arc ion plating, Appl. Surf. Sci. 258 (2012) 7047–7051.

[37] S.Y. Zhou, V.O. Pelenovich, B. Han, M.I. Yousaf, S.J. Yan, C.X. Tian, D.J. Fu, Effects of modulation period on microstructure, mechanical properties of TiBN/TiN nanomultilayered films deposited by multi arc ion plating, Vacuum 126 (2016) 34–40.
[38] M.M. Zhang, Y.X. Cheng, L. Xin, J.X. Su, Y.F. Li, S.L. Zhu, F.H. Wang, Cyclic oxidation behaviour of Ti/TiAlN composite multilayer coatings deposited on titanium alloy, Corros. Sci. 166 (2020), 108476.
[39] M.M. Zhang, L. Xin, X.Y. Ding, S.L. Zhu, F.H. Wang, Effects Ti/TiAlN composite multilayer coatings on corrosion resistance of titanium alloy in solid NaCl-H_2O-O_2 at 600 ℃, J. Alloy. Compd. 734 (2018) 307–317.
[40] Y.F. Ivanov, V.V. Shugurov, O.V. Krysina, E.A. Petrikova, O.V. Ivanova, O. S. Tolkachev, An electron-microscopy analysis of the gradient structure formed in titanium during deposition of a hard coating, Russ. Phys. J. 60 (2017) 875–883.
[41] S. Kumar, K. Chattopadhyay, G.S. Mahobia, V. Singh, Hot corrosion behaviour of Ti-6Al-4V modified by ultrasonic shot peening, Mater. Des. 110 (2016) 196–206.
[42] N. Eliaz, G. Shemesh, R.M. Latanision, Hot corrosion in gas turbine components, Eng. Fail. Anal. 9 (2002) 31–43.
[43] X. Chen, Q. An, S. Jiang, Y. Jiao, L.J. Huang, L. Geng, Revealing anti-oxidation mechanisms of titanium composite materials by detailed characterization of scale phase constitutions, Corros. Sci. 192 (2021), 109845.